Global NEST Journal, Vol 27, No 4, 07346

Development of ZrO_2-chitosan-hydroxyapatite nanocomposite films from Fish bone meal waste for biomedical applications

Kunduru Sumila Reddy[1], Randhi Uma Devi[2]* and Annapragada Ratnamala[2]*
[1]School of Science, GITAM University, Vishakhapatnam – 5300452, India
[1, 2]School of Science, GITAM University, Hyderabad Campus, Telangana State, 502329, India
Received: 05/02/2025, Accepted: 10/03/2025, Available online: 13/03/2025
*to whom all correspondence should be addressed: e-mail: urandhi@gitam.edu & rannapra@gitam.edu
https://doi.org/10.30955/gnj.07346

Graphical abstract

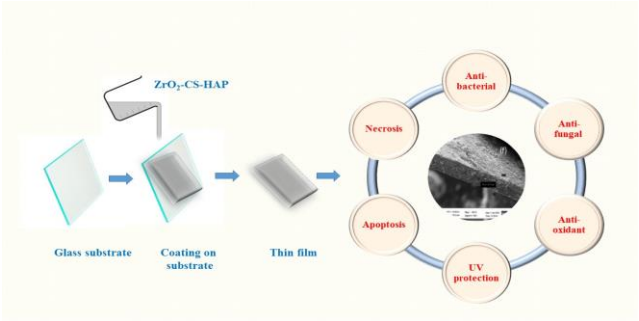

Abstract

This study describes a simple way for making films from natural sources, which is relevant since there is a rising demand for new materials that can make biocompatible films that are both effective and economical for use in biomedical applications. Fish bone waste and chitosan, a natural polymer used to manufacture thin films, are the sources of hydroxyapatites. The addition of zirconia (ZrO_2) to the thin films created a new nanocomposite known as ZrO_2-Chitosan-Hydroxyapatite (Zr-CS-HAP) films. These films demonstrated biocompatibility and have the potential to be produced in huge quantities. The structural, morphological, and biological studies were explored for possible biomedical applications like wound dressing, bone tissue regeneration, etc. The films showed good anti-oxidant and UV-protecting properties. Cytotoxicity of films by MTT test suggests that HeLa cell lines showed moderate to good cytotoxicity and better cervical properties. The films tested for Apoptosis-Necrosis in HeLa cells showed induced apoptosis of 52% and Necrosis of 21.3% in HeLa cells, similar to standard control.

Keywords: Chitosan, hydroxyapatite, cytotoxicity, anti-microbial susceptibility, apoptosis, necrosis

1. Introduction

Bioceramic materials used for knee, femur, hip, teeth, and other biological implants are designed to be highly absorbent and, in addition to their adequate load-bearing ability, can encourage the formation of natural bone tissue on the surfaces of artificial joints (Mythili *et al*. 2015). The creation of hybrid biomaterials with antibacterial, antifungal, anti-proliferative, and antioxidant capabilities is crucial for promoting quicker and more effective healing. In order to achieve superior orthopedic outcomes, an implant material must be mechanically and biologically sound and pass a corrosion-resistant test (Cunha *et al*. 2020). Metallic bio implant materials are essential in clinical applications because of their better mechanical qualities in physiological conditions. Hydroxyapatite [$Ca_{10}[PO_4]_6[OH]_2$], a calcium /phosphate-based bio-ceramic (Komal *et al*. 2020). chemically like an inorganic constituent of bone tissue and is non inflammatory, non immunogenic, biocompatible but also bioactive, has the ability to form a direct bond with living tissue (Fathi *et al*. 2008). It promotes tissue growth and is used as a prosthetic implant and filler material to replace damaged bones. Hydroxyapatite is promising for bone therapy, bone replacement, bone repair material, and wound dressing material (Rinaudo, 2006). Although HAP has a significant potential for wound healing because to its high biocompatibility and excellent angiogenic activity, traditional HAP materials are not suitable for wound dressing due to their high brittleness and poor mechanical qualities. However, the ability to add different dopants or reinforcements to HAP improves its qualities and expands its applications (Lansdown, 2002). Zirconium dioxide (ZrO_2) is a widely used material due to its excellent properties like biocompatibility, excellent mechanical strength, elastic modulus equivalent to that of bones, low stress, and high fracture toughness (Horti *et al*. 2020). Zirconia-based composite materials have superior corrosion resistance, high hardness, fracture toughness, and less magnetic susceptibility, making them useful for a variety of biomedical applications. One of the major components used in biomedicine is chitosan (CS), obtained by deacetylation from chitin, a natural polysaccharide found in crustacean shells. Chitosan has many biological properties, such as antibacterial, nontoxic, and biodegradable. The degree of deacetylation

(DDA) has a considerable impact on the solubility of chitosan. Chitosan is soluble up to a pH of 9 when its DDA is less than 40%. The Development and characterization of chitosan films were done to study the morphology and physical, mechanical, and degradation properties (Yang *et al*. 2010).

2. Methodology

Local market fish bones are defatted and deproteinized. Crushed bone species cleaned after 2 hours in acetone and heated to 250°C for six hours while stirring in a highly concentrated 4N sodium hydroxide solution with a 1:40 solid/liquid weight ratio. 20 g of bone powder in a crucible is heated at 650°C @ 5°C for 6 h and 950°C for 6 hours (Barakat *et al*. 2008). A beaker with 1M ammonium hydroxide contained the estimated amounts of $ZrOCl_2$, a precursor to ZrO_2, and bone powder to maintain pH 8. At 65–70°C, the mixture is stirred often. After washing and drying overnight at 45° C, the solid is calcined at 700° C for an hour. With vigorous stirring, Glacial acetic acid [1%v/v] dissolved chitosan at 25°C in 24 hours. Zr-HAP powder was added in various amounts after dissolving. A 0.5 N NaOH solution and distilled water rinse neutralized excess acetic acid. For film preparation, plasticizer glycerol was added and agitated at 40° C for 30 minutes to 60 mL. Glycerol as a plasticizer is added and swirled at 40° C for 30 minutes by eliminating air bubbles and particles to make the film. The solution was cast and evaporated onto a glass plate and dried for 72 h at 25 °C to form the film after 10 min of stirring at 40° C (Iline *et al*. 2022). Zr concentrations and weight percents are in **Table 1**. The prepared films were characterized with XRD, SEM, FTIR (Srinivasan *et al*. 2018). A calibrated digital Vernier Calliper-gauge micrometer measures film thickness. Five locations are measured and averaged for each film. Film microstructure and quality may change with doping (Gao, 2004). Porosity was measured using a standard approach (Khorasani *et al*. 2019). Each film was weighed before and after 60 minutes in dry ethanol until saturated.

Table 1. Details of the weight percentages of the components used in the preparation of the film

S.No	Sample Name	Chitosan (deacetylated)	Percentage ZrO_2 in Zr-HAP	Glycerol (mL)
1	Zr-CS-HAP-1 (Sample 1)	1% wt/v	1 wt/v % Zr on HAP	2.5
2	Zr-CS-HAP-2 (Sample 2)	1% wt/v	2 wt/v % Zr on HAP	3.5
3	Zr-CS-HAP-3 (Sample 3)	1% wt/v	3 wt/v % Zr on HAP	4.5
4	CS	1% wt/v	-	2.5
5	CS-HAP	1% wt/v	-	2.5

To assess swelling and water-uptake (WU%), 25 × 25 mm films were submerged in 5 mL of saline solution (NaCl 0.9% w/v) adjusted to pH 6.6. WU at 120 minutes was calculated using weight differential %. Hydrated samples were submerged in solution and baked at 60 °C for 24 hours to quantify erosion by weight. Erosion (E%) measures film weight loss in saline. For 24 h at 37 °C, the films were immersed in saline solution to measure disintegration and integrity.

2.1. Biological assessment

Human Cervix adenocarcinoma cell line HeLa is supplied from NCCS in Pune, India for film cytotoxicity. At 37°C with 5% CO_2 and 18–20% O_2, the cells were in DMEM with high glucose media, 10% FBS, and 1% antibiotic-antimycotic solution in a CO_2 incubator. Their subculture changed every two days. Colorimetric MTT cell proliferation assay used to measure cell proliferation and cytotoxicity (Gerlier and Thomasset, 1986). Antimicrobial susceptibility was tested on fungus (*Saccharomyces cerevisiae*), bacteria (*Escherichia coli*), and bacteria (*Staphylococcus aureus*). KIRBY Bauer Disc Diffusion showed a Zone of Inhibition for these species (Indumathi *et al*. 2019). To measure film antimicrobial activity, overnight liquid cultures of selected bacteria were diluted with 1 g L-1 peptone and 8.5g L-1 sodium chloride. UV light sterilized 1.3 cm CS and Zr-CS-HAP film discs for 10 minutes. To each disk in a sterile tube, 200µl of liquid inoculum was added. The films were inoculated for 0, 2, 4, and 6 hours at 37 °C. Each tube was diluted with 1.8 mL peptone water (Tabassum *et al*. 2021). We cultivated 20 µl aliquots of each diluted solution on Muller Hinton Agar at 37 °C before counting colonies. A triple statistical analysis was performed on each experiment (Raphael and Meimandipor, 2017). Two samples of Zr-CS-HAP -2 and -3 were tested for antioxidant activity using DPPH free radical scavenging (McDonald *et al*. 2006). Apoptosis, Necrosis, and other types of cell death were characterised by the expression of phosphatidylserine on the cell surface, which is detected by using Annexin-V as a probe (Homburg *et al*. 1995). Thus, viable, early apoptotic, late apoptotic, and necrotic cells are represented by the populations Annex-V-/IP-, Annex-V+/IP, Annex-V+/IP+, and Annex-V-/IP+, respectively (Obrien and Bolton, 1995). Following staining, propidium iodide is represented by the pink stain and Annexin V by the green stain. The yellow tetrazolium dye MTT is reduced to formazan crystals by the MTT Assay test, which can be used to measure cytotoxicity and cell proliferation. To evaluate viability, the MTT test (3-[4,5-dimethyl-2-thiazol]-2,5-diphenyl-2H-tetrazolium bromide) was employed.

3. Results and discussion

XRD can determine Zr-CS-HAP's crystal structure and microstructure orientation using the thin film detector. XRD patterns show strong crystallinity, ZrO_2, HAP, and Chitosan peaks. Zr-CS-HAP diffraction peaks display the tetragonal phase of ZrO_2, coinciding with JCPDS card no.

89-7710, with a significant peak at 2ɵ value 30.0°, corresponding to the (101) plane. HAP peaks at 2Θ values of 26.0° (002), 32.2° (211), 40.1° (310), and 45.9° (222) match the hexagonal structure of hydroxy apatite and JCPDS card no 09-0432 (Ashkezari *et al*. 2023). Chitosan had low peaks at 2 theta 15, 20.0°, and 36.7°, as before (R pallela *et al*. 2012). FTIR functional groups of the composite film are presented in **Figure 1**. O-H stretching causes the spectrum's big peak at 3385 cm−1. Chitosan amine peaks at 1629 cm−1 (Madeha and Ntanoyenkosi, 2024). Peaks at 567, 1055, and 1566 cm−1 (phosphate groups) indicate HAP (Panda *et al*. 2003). Spectrum data at 854, 1,413, and 1,451 cm-1 suggests carbonate ions. Also observed are Zr-O stretching peaks at 466 and 434. The spectrum shows all ZrO_2, Chitosan, and HAP peaks. A Labsphere UV-2000F ultraviolet transmittance tester measured a few films' UPF (Balraj *et al*. 2017). **Figure 1** depicts Zr-CS-HAP UV-visible diffuse reflectance spectra with various zirconia loadings. Figure shows absorption is concentrated at 308, 316, and 330 nm. Valence band to conduction band transition may explain this. ZrO_2 nanosheets displayed no extrinsic states and a high peak at 319 and 330 nm, according to literature. This suggested minor ZrO_2 nanosheet surface defects (Fatemh and Mohammad, 2014).

A calibrated digital Vernier Calliper-gauge micrometer measures film thickness at five locations for each film and calculates the average. Doping could alter film quality and microstructure. **Table 2** shows the weights of the films before and after 60 minutes in dry ethanol till saturated. SEM micrographs of zirconia loaded on HAP films at different magnifications are shown in **Figure 2**. Figures (2a) and (2b) show just chitosan film, (2c) and (2d) show rod-shaped CS-HAP films, and (2e) and (2f) exhibit Zr-CS-HAP films. Homogeneous films with considerable ZrO_2 dispersion or nanofibers embedded in HAP films. SEM images reveal a film thickness of 14-49 µm. These values match vernier caliper measurements. **Figure 3** illustrates EDAX pattern and metal % at a given time.

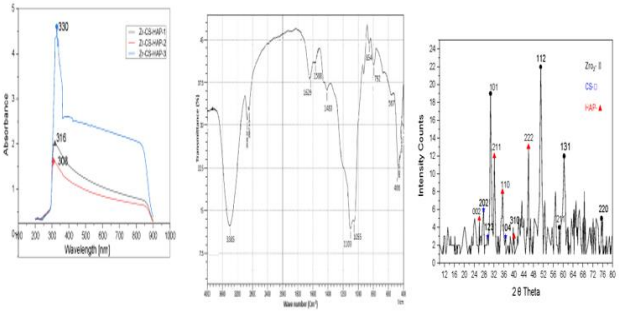

Figure 1. UV-Vis DRS spectra, FTIR and XRD of Zr-CS-HAP thin films

Table 2. Details of thickness, porosity, and UPF values critical wavelength and percentage transmittance

Sample Name	Thickness (mm)	Porosity (%)	Water uptake/time min^{-1}(%)	% Erosion	Water uptake %/min	UPF value	UPF rating	T UVA%	T UVA%
Zr-CS-HAP-1	0.025	26.61	1.6	50.0	2.9	153.38	excellent	0.57	2.25
Zr-CS-HAP-2	0.019	28.51	1.7	51.1	2.9	155.26	excellent	0.73	2.16
Zr-CS-HAP-3	0.020	29.78	2.2	52.3	2.5	140.15	excellent	0.31	2.21
CS	0.036	20.27	1.0	40	2.4	19.09	poor	0.68	2.27
CS-HAP	0.09	22.81	3.2	66	2.5	15.9	poor	0.65	2.31

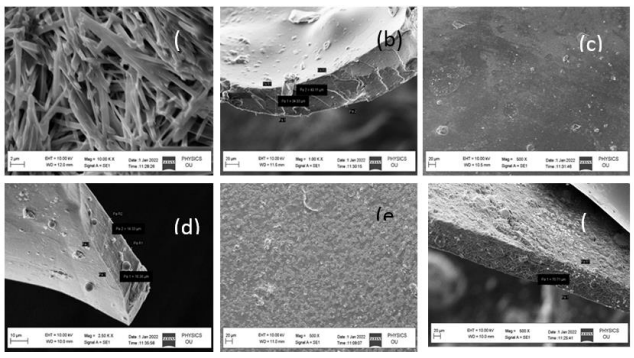

Figure 2. Scanning Electron Microscopes. (2a) & (2b) chitosan film (2c) & (2d) CS-HAP, (2e) & (2f) Zr-CS-HAP

3.1. MTT assay

Cytotoxicity should not be exhibited by biomaterials used in biological applications. Using an MTT assay, Zr-CS-HAP thin films were examined in vitro to determine the nontoxic concentration. This MTT (3-[4,5-dimethylthiazol-2-yl]-2,5 diphenyl tetrazolium bromide) assay, measures mitochondrial activity by watching how cells transform MTT into formazan crystals while they are still alive. The capacity of metabolically active cells to transform MTT into formazan crystals was assessed. Based on the observations in Statistical data of cell cytotoxicity study by MTT assay, it is suggesting that against HeLa cell lines, Test Compounds, namely Zr-CS-HAP-2 and Zr-CS-HAP-3 showing moderate cytotoxic potential properties with the IC_{50} Concentrations of 280µg/mL and 519µg/mL respectively. To demonstrate the mechanism of action of films on human cervical cancer cells, more research was conducted, including investigations on the cell cycle using PI staining, apoptosis using Annexin V/PI staining, apoptotic protein expressions such as Caspase 3,7,9, Bcl2, p53, and ROS.

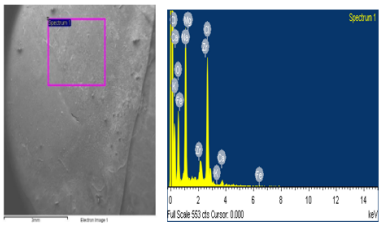

Element	Weight %	Atomic wt.%
O	29.21	44.47
Na	22.99	24.36
Mg	0.33	0.33
P	39.49	27.13
K	0.46	0.28
Ca	3.52	2.14
Fe	1.21	0.53
Zr	2.80	0.75
Totals	100.00	

Figure 3. An EDAX Pattern of Zr-CS-HAP and a percentage of metal at a particular point

It is acknowledged in the literature that CS is nontoxic, and the incorporation of HAP induces proliferative properties (Koopman *et al.* 1994). Moreover, the ZrO_2 was also reported to be bioinert, and these coatings were expected to improve the interaction with cells and tissues. The proliferation of the cells is due to the presence of calcium in hydroxyapatite. Calcium-sensing receptors trigger chemotaxis and proliferation in response to elevated extracellular calcium levels. In this regard, Zr-CS-HAP would be more beneficial because calcium can encourage development and proliferation through the mechanical strength of Zr-based ceramics.

3.2. Anti-microbial susceptibility

The antibacterial activity of Zr-CS-HAP films was evaluated against three different microbiological strains to see whether the powder's absorption into the film affected the behavior of Zirconium and HAP. The disc diffusion method and viable cell count assay measured the films' antibacterial and antifungal properties. The Zr-CS-HAP films repressed *Escherichia Coli* Gram Negative, *Staphylococcus aureus* Gram Positive, and *Saccharomyces cerevisiae*. **Table 3** lists the species and zone of inhibition. Films with less Zr-CS-HAP have smaller inhibition zones. How well the inoculum kills germs depends on its concentration. Gram-positive bacteria show no influence from Zr-HAP in the film (**Figure 4a**). Staphylococcus aureus may be resistant to Chitosan films with a 1.5 log unit reduction. The regular Chitosan film and Zr-HAP film differ slightly yet considerably. **Figure 4b** targets Gram-negative *E. coli*. Both examples had two log units fewer live bacteria after two hours with UV-absorbing powder in their matrix, proving that the CS film is still effective against bacteria. A small shift occurred after 4 hours, and both samples reached 5 log CFU/mL after 6 hours. As with other antibacterial coatings, a modest uptick suggests weak microbial return. Although the bacterial population has grown, it is still modest. A *Saccharomyces cerevisiae* test on the CS film showed just a slight decrease in active microorganisms (**Figure 4c**), ruling out considerable action. Live cells increased after 6 hours as the Zr-CS-HAP film grew. Fungal activity-promoting compounds may be released during incubation. The elements may be organic bits or molecules. Although the chemicals have been revealed in organism tests, the CS matrix's high antibacterial activity may have hidden their benefits. But additional investigation is needed. Overall, Zr-CS-HAP films have outstanding Gram-positive and Gram-negative antibacterial activity, peaking between 2 and 4 hours. Good wound dressings, Zr-CS-HAP films absorb UV radiation and are antibacterial (**Table 4**).

Table 3. Details of the Microorganisms Used and Zone of Inhibition

S.No	Name of the Microorganisms	Antibiotic Disc	Zone of Inhibition
1	*Escherichia Coli*	Control Zr-CS-HAP –2 Zr-CS-HAP –3	Nil 1.5 mm 1.8 mm
2	*Staphylococcus aureus*	Control Zr-CS-HAP- 2 Zr-CS-HAP- 3	Nil 1.0 mm 1.0 mm
3	*Saccharomyces Cerevisiae*	Control Zr-CS-HAP- 2 Zr-CS-HAP- 3	Nil 1.0 mm 1.6 mm

Table 4. Comparative DPPH % inhibition in a dose-dependent manner

Concentration (µg/mL)	Zr-CS-HAP-2	Zr-CS-HAP-3
DPPH alone	0	0
Ascorbic acid-10	44.45	44.45
62.5	4.45	0.13
125	8.58	2.22
250	13.44	6.95
500	30.87	10.40
1000	73.44	55.27

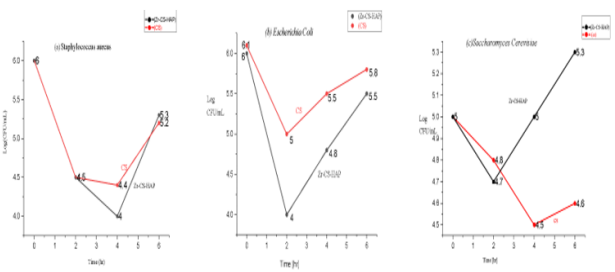

Figure 4 (a) Antimicrobial assay of simple chitosan (CS) and chitosan with Zr-HAP powder (Zr-CS-HAP-2) film capacity to inactivate Gram-positive bacteria

3.3. DPPH RSA

The CS-Zr-HAP films were studied for DPPH radical scavenging (RSA). The 2,2, diphenyl-picrylhydrazyl (DPPH) technique has several medicinal and food-related uses. Antioxidant activity of chemicals, especially phenolic compounds, can be evaluated using this approach. The Spectrophotometer/ELISA reader's observations in the

statistical results of the DPPH RSA study show that the test compounds Zr-CS-HAP-2 and Zr-CS-HAP-3, inhibited DPPH RSA in a dose-dependent manner with IC50 values of 663 µg/mL and 993µg/mL, respectively (**Figure 5**). The standard control for the study was ascorbic acid. The measured DPPH radical scavenging conclusions of the tested compounds (Zr-CS-HAP-3) reveal that they have significant dose-dependent DPPH radical scavenging potency, while Zr-CS-HAP-2 and other samples have moderate DPPH radical scavenging activity. Ascorbic acid & Zr-CS-HAP-2 both showed notable DPPH radical scavenging efficacy in a dose-dependent manner (Ngugen *et al.* 2022) (**Table 5**).

3.4. Apoptosis and necrosis

Annexin V/PI double labelling was used to quantify cell apoptosis and necrosis, and the results are displayed in **Figure. 5**. When compared to the control group, the Zr-CS-HAP-2-treated cells showed variable levels of necrosis instead of apoptosis. In late apoptosis or when the treatment period was prolonged, the necrosis rates of the Zr-CS-HAP-2-treated cells rose from 21.35% to 43.11%. (A) % live, apoptosis and necrotic population observed in HeLa cells treated with culture medium alone (Untreated), (B) Camptothecin and Test compound,(C) Zr-CS-HAP-2, with 72.83µg/mL concentration (D) Quadrant plots showing the % of HeLa cells that are alive, in apoptosis, and necrotic after being subjected to the amounts of Camptothecin (3.8 µM/mL), Test compound, Zr-CS-HAP-2, and culture media alone (Untreated), respectively.

Table 5. Apoptosis and necrosis assay of cells exposed to Zr-CS-HAP-2 films

% population of cells	Necrosis	Late apoptosis	Live	Early apoptosis
Untreated	0	0.72	98.85	0.43
Camptothecin-3.8µM/mL	0.19	52.82	28.81	18.18
Zr-CS-HAP- 2 with 72.83µg/mL	21.35	8.93	26.61	43.11

The above graph and table clearly show that the study's Std control drug Camptothecin, the test substance Zr-CS-HAP-2, significantly increased the amount of apoptosis (52%) and necrosis (21.35%) in HeLa cells.

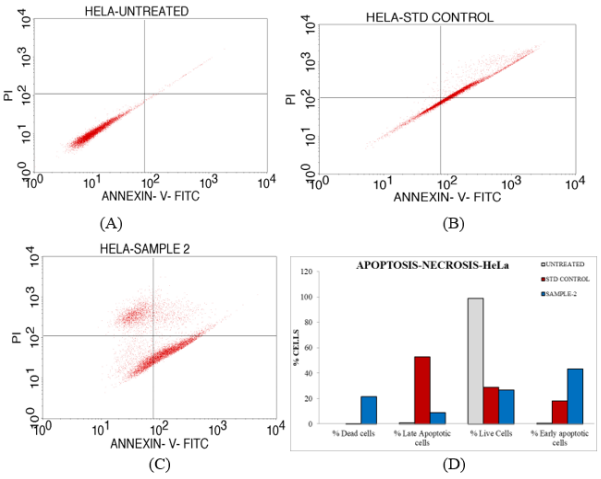

Figure 5. Apoptosis and Necrosis results

4. Conclusions

Chitosan, ZrO_2 HAP-based hybrid films were successfully prepared. The characteristics of these films indicate that they are suitable for biomedical applications like wound dressings because they help to reduce bacterial infections and bone tissue engineering applications. MTT assay, DPPH, Apoptosis, and Necrosis studies also state that the Zr-CS-HAP-2 films have an impact and possibility to explore in bone tissue engineering applications. Between two and four hours, the Zr-CS-HAP films exhibit the highest level of antibacterial activity against both Gram-positive and Gram-negative pathogens. The fungal organism *Saccharomyces Cerevisiae* has been demonstrated to be mildly affected by Zr-CS-HAP film. Its bioactivity, biodegradability, and biocompatibility make it highly beneficial in many scientific domains.

References

Al-Kelani M. and Buthelezi N. (2024). Advancements in medical research: Exploring Fourier Transform Infrared (FTIR) spectroscopy for tissue, cell, and hair sample analysis, *Skin Research and Technology* 2024, https://doi.org/10.1111/srt.13733

Ashkezari S., MaryamSadat A. and SattariZahra. (2023). Antibiotic and inorganic nanoparticles co-loaded into carboxymethyl chitosan-functionalized niosome: Synergistic enhanced antibacterial and anti-biofilm activities, *Journal of Drug Delivery Science and Technology*, **83**, 104386. https://doi.org/10.1016/j.jddst.2023.104386

Balraj B., Arulmozhi M., Siva C. and Krithikadevi R. (2017). Synthesis, characterization and electrochemical analysis of hydrothermal synthesized AgO incorporated ZrO2 nanostructures, *Journal of Materials Science: Materials in Electronics*, **28**(8), 5906–5912. https://doi.org/10.1007/s10854-016-6264-9

Barakat N.A.M., Khalil K.A. and Sheikh F.A. (2008). Physiochemical characterizations of hydroxyapatite extracted from bovine bones by three different methods: Extraction of biologically desirable HAP. *Materials Science and Engineering: C*, **28**(8), 1381–1387. https://doi.org/10.1016/j.msec.2008.03.003

Cunha C.S., Castro P.J., Sousa S.C. and Pullar R.C. (2020), Films of chitosan and natural modified hydroxyapatite as effective UV-protecting, biocompatible and antibacterial wound dressings. *International journal of biological macromolecules*, **159**, 1177–1185. https://doi.org/10.1016/j.ijbiomac.2020.05.077

Fatemeh D. and Estarki M.R. (2014). Synthesis and optical properties of pure monoclinic zirconia nanosheets by a new

precursor, *Ceramics International*, **40**(6), 8427–8433. https://doi.org/10.1016/j.ceramint.2014.01.052

Fathi M.H, Hanifi A. and Mortazavi V. (2008), Preparation and bioactivity evaluation of bone-like hydroxyapatite nanopowder. *Journal of Materials Processing Technology*, **202**(1–3), 536–542. https://doi.org/10.1016/j.jmatprotec.2007.10.004

Gao W.L. (2004), ZnO thin films produced by magnetron sputtering. **30**(7), 1155–1159. https://doi.org/10.1016/j.ceramint.2003.12.197

Gerlier D. and Thomasset N. (1986), Use of MTT colorimetric assay to measure cell activation. *Journal of immunological methods*, **94**(1–2), 57–63. https://doi.org/10.1016/0022-1759(86)90215-2

Homburg C.H., De Haas M. and Von Dem Borne A.E. (1995). Human Neutrophils Lose Their Surface Fc Gamma RIII and Acquire Annexin V Binding Sites During Apoptosis In Vitro. *Blood*, **85**(2), 532–540. https://doi.org/10.1182/blood.V85.2.532.532

Horti N.C., Kamatagi M.D., Nataraj S.K., Wari M.N. and Inamdar S.R. (2020). Structural and optical properties of zirconium oxide (ZrO2) nanoparticles: effect of calcination temperature, *Nano Express*, **1**(1), 010022. DOI: 10.1088/2632-959X/AB8684

Iline-Vul T., Kanovsky N., Yom-Tov D., Nadav-Tsubery M. and Margel S. (2022), Design of silane-based UV-absorbing thin coatings on polyethylene films, Colloids and Surfaces A: *Physicochemical and Engineering Aspects*, **648**, 129164. https://doi.org/10.1016/j.colsurfa.2022.129164

Indumathi M.P., Sarojini K.S. and Raja Rajeswari G.R. (2019). Antimicrobial and biodegradable chitosan/cellulose acetate phthalate/ZnO nano composite films with optimal oxygen permeability and hydrophobicity for extending the shelf life of black grape fruits. *International Journal of Biological Macromolecules*, **132**, 1112–1120. https://doi.org/10.1016/j.ijbiomac.2019.03.171

Khorasani M.T, Joorabloo A., Adeli H., Mansoori-Moghadam Z. and Moghaddam A. (2019). Design and optimization of process parameters of polyvinyl (alcohol)/chitosan/nano zinc oxide hydrogels as wound healing materials. Carbohydrate Polymers, **207**, 542–554. https://doi.org/10.1016/j.carbpol.2018.12.021

Komal P.M., Regmi S. and Nepal A. (2020), Extraction and Characterization of Novel Natural Hydroxyapatite Bioceramic by Thermal Decomposition of Waste Ostrich Bone. *International Journal of Biomaterials*. ArticleID 1690178. https://doi.org/10.1155/2020/1690178

Koopman G., Reutelingsperger C.P. and Kuijten G.A. (1994). Rapid Communication Annexin V for flow cytometric detection of phosphatidylserine expression on B cell undergoing apoptosis. *Blood* **84** (5), 1415–1420. https://doi.org/10.1182/blood.V84.5.1415.1415

Lansdown A.B.G. (2002). Calcium: a potential central regulator in wound healing in the skin. *Wound repair and regeneration* **10** (5), 271–285. https://doi.org/10.1046/j.1524-475X.2002.10502.x

MacDonald-Wicks L.K., Wood L.G. and Garg M.L. (2006). Methodology for the determination of biological antioxidant capacity in vitro: a review. *Journal of the Science of Food and Agriculture*, **86**(13), 2046–2056. https://doi.org/10.1002/jsfa.2603

O'Brien M.C. and Bolton W E. (1995). Comparison of cell viability probes compatible with fixation and permeabilization for combined surface and intracellular staining in flow cytometry. *Journal of Quantitative cell science*, **19**(3), 243–255. https://doi.org/10.1002/cyto.990190308

Pallela R., Venkatesan J., Janapala V.R. and Kim S.K. (2012). Bio physicochemical evaluation of chitosan hydroxyapatite-marine sponge collagen composite for bone tissue engineering. *Journal of Biomedical Materials Research Part A* :100A, 486–495. https://doi.org/10.1002/jbm.a.33292

Panda R.N., Hsieh M.F., Chung R.J. and Chin T.S. (2003). FTIR, XRD, SEM and solid state. NMR investigations of carbonate-containing hydroxyapatite nano-particles synthesized by hydroxide-gel technique, *Journal of Physics and Chemistry of Solids*, **64**(2), 193–199. https://doi.org/10.1016/S0022-3697(02)00257-3

Prakasam M., Locs J. and Salma-Ancane K. (2015), Fabrication, properties and applications of dense hydroxyapatite: A review. *Journal of functional Biomaterials*, **6**(4), 1099–1140. https://doi.org/10.3390/jfb6041099

Raphaël K.J. and Meimandipour A. (2017). Antimicrobial Activity of Chitosan Film Forming Solution Enriched with Essential Oils; an in Vitro Assay. *Iranian Journal of Biotechnology*, **15**(2), 111–119. https://doi.org/10.15171/ijb.1360

Rinaudo M. (2006). Chitin and chitosan: Properties and applications. *Progress in Polymer Science*, **31**(7), 603–632. https://doi.org/10.1016/j.progpolymsci.2006.06.001

Srinivasan H., Kanayairam V. and Ravichandran R. (2018), Chitin and chitosan preparation from shrimp shells Penaeus monodon and its human ovarian cancer cell line, PA-1, *International Journal of Biological Macromolecules*, **107**, 66–2667. https://doi.org/10.1016/j.ijbiomac.2017.09.035

Tabassum N., Kumar D., Verma D., Bohara R.A. and Singh M.P. (2021). Zirconium oxide (ZrO2) nanoparticles from antibacterial activity to cytotoxicity: A next Generation of multifunctional nanoparticles, *Materials Today Communications*, **26**, 102156. https://doi.org/10.1016/j.mtcomm.2021.102156

Thao N.M.T., Van Tri H. and Han T.N. (2022), Measure the ultraviolets protection factor (UPF) of Fabrics on UV-Vis spectrophotometer, *Journal of Science Technology and Food* **22**(3), 321–329.

Yang Y., Liu C., Wu H. and Li R. (2010). Preparation and characterization of films based on zirconium sulfophenyl phosphonate and chitosan, *Carbohydrate research*, **345**(1), 148-153. DOI: 10.1016/J.CARRES.2009.10.012.